AGU PUBLICATIONS

JGR

Journal of Geophysical Research: Planets

RESEARCH ARTICLE
10.1002/2016JE005071

Tidal deformation of Ganymede: Sensitivity of Love numbers on the interior structure

Shunichi Kamata[1], Jun Kimura[2], Koji Matsumoto[3,4], Francis Nimmo[5], Kiyoshi Kuramoto[6], and Noriyuki Namiki[7]

[1]Creative Research Institution, Hokkaido University, Sapporo, Japan, [2]Earth-Life Science Institute, Tokyo Institute of Technology, Tokyo, Japan, [3]RISE Project Office, National Astronomical Observatory of Japan, Oshu, Japan, [4]Department of Astronomical Science, Graduate University for Advanced Studies (SOKENDAI), Mitaka, Japan, [5]Department of Earth and Planetary Sciences, University of California, Santa Cruz, California, USA, [6]Department of Cosmosciences, Hokkaido University, Sapporo, Japan, [7]RISE Project Office, National Astronomical Observatory of Japan, Mitaka, Japan

Key Points:
- Tidal Love numbers h_2 and k_2 of Ganymede are calculated under different parameter conditions
- Phase lag detection is important for inferring the presence/absence of a subsurface ocean
- Uncertainty in the shell thickness can be reduced if both h_2 and k_2 are measured

Correspondence to:
S. Kamata,
kamata@mail.sci.hokudai.ac.jp

Citation:
Kamata, S., J. Kimura, K. Matsumoto, F. Nimmo, K. Kuramoto, and N. Namiki (2016), Tidal deformation of Ganymede: Sensitivity of Love numbers on the interior structure, *J. Geophys. Res. Planets*, *121*, 1362–1375, doi:10.1002/2016JE005071.

Received 8 MAY 2016
Accepted 10 JUL 2016
Accepted article online 13 JUL 2016
Published online 28 JUL 2016

Abstract Tidal deformation of icy satellites provides crucial information on their subsurface structures. In this study, we investigate the parameter dependence of the tidal displacement and potential Love numbers (i.e., h_2 and k_2, respectively) of Ganymede. Our results indicate that Love numbers for Ganymede models without a subsurface ocean are not necessarily smaller than those with a subsurface ocean. The phase lag, however, depends primarily on the presence/absence of a subsurface ocean. Thus, the determination of the phase lag would be of importance to infer whether Ganymede possesses a subsurface ocean or not based only on geodetic measurements. Our results also indicate that the major control on Love numbers is the thickness of the ice shell if Ganymede possesses a subsurface ocean. This result, however, does not necessarily indicate that measurement of either of h_2 or k_2 alone is sufficient to estimate the shell thickness; while a thin shell leads to large h_2 and k_2 independent of parameters, a thick shell does not necessarily lead to small h_2 and k_2. We found that to reduce the uncertainty in the shell thickness, constraining k_2 in addition to h_2 is necessary, highlighting the importance of collaborative analyses of topography and gravity field data.

1. Introduction

Investigating whether the icy satellites of giant planets possess subsurface oceans or not is crucial not only to reveal their thermal histories but also to understand their astrobiological potential. In terms of this, Ganymede, a Jovian icy satellite, is an interesting body. Theoretical studies have shown that the presence of a subsurface ocean in current Ganymede can be strongly controlled by the composition of the ocean; a pure H_2O ocean would have frozen by the present [e.g., *Spohn and Schubert*, 2003; *Bland et al.*, 2009; *Kimura et al.*, 2009], while an ocean containing other components such as salts and/or ammonia may persist to the present because of its lower melting point [e.g., *Sotin and Tobie*, 2004]. The interior thermal state would be coupled with the orbital evolution because tidal heating is a potential internal heat source. Although the orbital state of present Ganymede leads to only a negligibly low tidal heating rate [e.g., *Hussmann et al.*, 2010], that of past Ganymede may lead to a higher tidal heating rate; Ganymede may have passed through one or more Laplace-like resonances that were able to pump the orbital eccentricity, supporting the development of a subsurface ocean [*Showman et al.*, 1997; *Bland et al.*, 2009]. While theoretical studies propose different scenarios and different present-day interior structure models, previous observations support the presence of a subsurface ocean in Ganymede indirectly; magnetometer data from the Galileo spacecraft suggest the presence of a subsurface ocean with dissolved electrolytes at a depth of the order of 150 km [*Kivelson et al.*, 2002]. Recent observations of auroral ovals of Ganymede using the Hubble Space Telescope also suggest the presence of an electrically conductive subsurface ocean [*Saur et al.*, 2015]. Nevertheless, more direct observational evidence is necessary to definitively infer the presence/absence of a subsurface ocean in Ganymede and determine its depth and volume.

In 2030s, Jupiter Icy Moons Explorer (JUICE) will orbit Ganymede carrying multiple scientific instruments to reveal the environment, surface, and interior of Ganymede [e.g., *Grasset et al.*, 2013]. During the mission lifetime, Ganymede Laser Altimeter (GALA) on board the JUICE spacecraft will make multiple measurements at many geographically fixed locations to provide a time series of surface displacement [*Steinbrügge et al.*, 2015].

Considering Ganymede's nonzero eccentricity, the temporal changes of the surface displacement are likely to be due to tidal deformation. In addition, precise radio tracking of the JUICE spacecraft would provide the tidal signal of Ganymede's gravity field [*Parisi et al.*, 2014]. Since the presence/absence of a subsurface ocean largely affects tidal response [e.g., *Moore and Schubert*, 2003], tidal deformation measurements through laser altimetry and the radio science experiment are key observations to constrain the interior structure of Ganymede [*Grasset et al.*, 2013].

There are several issues that should be addressed in anticipation of such observations. First, what kind of data is the most effective to determine the presence/absence of a subsurface ocean? If Ganymede possesses a subsurface ocean, with what precision can we constrain the thickness of the ice shell? These issues require numerical studies using realistic interior models under a wide variety of parameter conditions. Although the tidal response of Ganymede has already been investigated by several authors, previous models generally made simplifying assumptions. For example, the models used by *Moore and Schubert* [2003] ignore the strong temperature dependence of ice viscosity, and those by *Steinbrügge et al.* [2015] assume a fully elastic model. Another study using 3-D modeling by *A et al.* [2014] adopts a depth-dependent viscosity profile, though the parameter ranges investigated are limited. While the factors which are not incorporated in previous studies may not be the dominant effects on the tidal response of Ganymede, such effects should be quantified using a realistic model in order to extract quantitative information on the interior structure from tidal deformation measurements. Furthermore, these previous studies consider the amplitude but not the phase lag of tidal response; whether additional constraints on the interior structure can be obtained from the latter quantity has not been examined hitherto.

In this study, we calculate the amplitude and phase lag of tidal deformation under a wide variety of parameter conditions (i.e., ice viscosity, ice rigidity, and shell thickness) and investigate the major controls on the tidal response of Ganymede. We consider cases with and without a subsurface ocean. Sections 2 and 3 describe the numerical calculation models and method adopted, respectively. Section 4 presents results obtained and discusses implications for future geodetic observations.

2. Model

In this study, we adopt a 1-D, fully differentiated Ganymede model consisting of an outer H_2O layer, a rocky mantle, and a metallic core. The H_2O layer is further divided into several layers depending on pressure, as discussed below. The solid H_2O layers and the rocky mantle are assumed to be Maxwellian viscoelastic bodies, and the subsurface ocean and the core are assumed to be inviscid fluids, respectively. Table 1 lists parameters adopted. Free parameters are the thickness of the ice Ih shell D_{sh}, the rigidity of the shell μ_{sh}, the reference viscosity for the shell (i.e., the viscosity at the melting point) η_{ref}, and the viscosity of high-pressure (HP) ices. Although lateral variations in physical properties are not considered, such variations have little effect on the degree-2 tidal deformation for Ganymede [*A et al.*, 2014].

2.1. Density and Bulk Moduli

We model the density profile for the H_2O layer based on the thermodynamic model for water and ices by *Choukroun and Grasset* [2010]. We assume that the surface layer consists of ice Ih. Assuming that the satellite is in hydrostatic equilibrium, we integrate

$$\frac{dP}{dr} = -\rho(P)g(r) \tag{1}$$

$$\frac{dg}{dr} = 4\pi G\rho(P) - \frac{2g(r)}{r} \tag{2}$$

from the surface to the bottom of the ice Ih shell. Here P is pressure, ρ is density, g is gravitational acceleration, r is radial distance from the center of the satellite, and G is the gravitational constant, respectively. We ignore the temperature dependence of density for ice Ih while incorporating its pressure dependence since the former is extremely small while the latter can be up to several percent. The density profile gives the bulk modulus profile via the Adams-Williamson condition:

$$\frac{d\rho}{dr} + \rho^2(r)\frac{g(r)}{\kappa(r)} = 0, \tag{3}$$

where κ is bulk modulus.

Table 1. Model Parameters[a]

Symbol	Quantity	Value	Unit
R_s	Radius of Ganymede	2631.2	km
$\bar{\rho}$	Mean density	1942	kg m^{-3}
C/MR^2	Normalized moment of inertia	0.3115	Dimensionless
D_{sh}	Thickness of the ice Ih layer	1–155.25	km
ρ_m	Density of the rocky mantle	3222	kg m^{-3}
ρ_c	Density of the metallic core	5330	kg m^{-3}
η_{ref}	Reference viscosity of ice Ih	10^{12}–10^{17}	Pa s
η_{oc}	Viscosity of the ocean	0	Pa s
η_{III}	Viscosity of ice III	10^{12}–10^{17}	Pa s
η_{V}	Viscosity of ice V	10^{12}–10^{17}	Pa s
η_{VI}	Viscosity of ice VI	10^{12}–10^{17}	Pa s
η_m	Viscosity of the rocky mantle	10^{21}	Pa s
η_c	Viscosity of the metallic core	0	Pa s
E_a	Activation energy of ice Ih	60	kJ mol^{-1}
T_s	Surface temperature	110	K
k	Thermal conductivity of ice Ih	2.5	W m^{-1} K^{-1}
C_p	Specific heat of ice Ih	2000	J kg^{-1} K^{-1}
α_v	Thermal expansivity of ice Ih	1.4×10^{-4}	K^{-1}
μ_{sh}	Rigidity of ice Ih	0.1–10	GPa
μ_{oc}	Rigidity of the ocean	0	GPa
μ_{III}	Rigidity of ice III	4.6	GPa
μ_{V}	Rigidity of ice V	6.1	GPa
μ_{VI}	Rigidity of ice VI	7.5	GPa
μ_m	Rigidity of the rocky mantle	82	GPa
μ_c	Rigidity of the metallic core	0	GPa
$2\pi/\omega$	Orbital period	7.155	day
n	Spherical harmonic degree	2	Dimensionless

[a]Based on *Schubert et al.* [2004], *Lewis* [1995], and *Sohl et al.* [2002].

The basal temperature (i.e., the melting point) T_m of the ice Ih shell can be determined from the pressure P at the base of the shell. We assume that the subsurface ocean layer has an adiabatic temperature profile:

$$\frac{dT}{dr} = -\frac{\alpha_v(T)g(r)}{C_p(T)}T, \tag{4}$$

where T is temperature, α_v is thermal expansivity, and C_p is specific heat, respectively. We integrate equation (4) as well as equations (1) and (2) in the ocean layer. The values for $\alpha_v(T)$ and $C_p(T)$ are calculated from the formulation by *Choukroun and Grasset* [2010]. We compare this *P-T* curve for the ocean layer and the melting curve of HP ices and determine the thickness of the ocean. Results are shown in Figure 1, indicating that the temperature increase in the subsurface ocean can be up to >10 K and leads to a thicker ocean.

In a similar manner to the ice Ih layer, we integrate equations (1) and (2) for HP ice layers and determine the phase boundary between ice III, ice V, and ice VI. Note that the presence of ice III and ice V layers depends on the *P-T* curve of the ocean (thus depends on D_{sh}), while the ice VI layer appears under all calculation conditions (see Figure 1).

The determination of the depth of the boundary between the ice VI layer and the rocky mantle and that between the rocky mantle and the metallic core require additional assumptions. For our nominal model, we use a mantle density ρ_m of 3222 kg m^{-3}, which is for olivine, and a core density ρ_c of 5330 kg m^{-3}, which is for Fe-FeS [*Sohl et al.*, 2002]. Under these assumptions, only two parameters remain to be determined: the radius of the silicate mantle and that of the metallic core. These values are chosen to satisfy two gravitational constraints: the mean density and the normalized moment of inertia given by *Schubert et al.* [2004] (see Table 1).

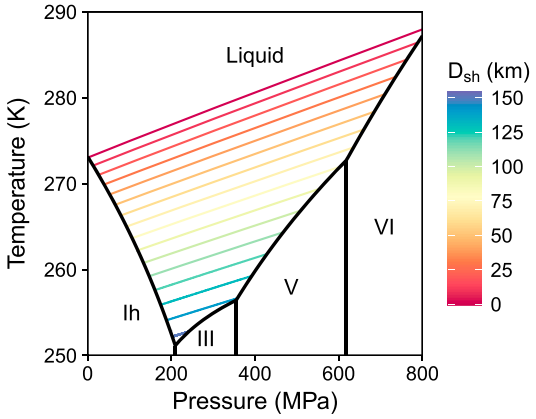

Figure 1. Phase diagram of H_2O [*Choukroun and Grasset*, 2010]. Colored lines show temperature profiles of our models for different shell thicknesses (D_{sh}). A thinner shell has a higher ocean temperature, leading to a thicker ocean.

Note that we ignore the pressure dependence of densities for mantle and core. To maintain consistency in our model, bulk moduli for these two deepest layers are assumed to be infinite (cf. equation (3)).

Figure 2 shows our interior structure model obtained through the procedures described above. The maximum shell thickness is found to be ~155 km, which is much thinner than that modeled by *Steinbrügge et al.* [2015]. This is simply because the work by *Steinbrügge et al.* [2015] does not consider the phase diagram of H_2O in detail. The most uncertain parameter is the density of the core. We adopt a conservative value for core density, though the actual core density may be that of pure Fe: ~8000 kg m^{-3} [e.g., *Schubert et al.*, 2004]. Although such a large density leads to a significantly smaller core, as clearly seen in Figure 2, tidal response depends little on the deep interior structure. We found that the difference between Love numbers for our nominal model (i.e., $\rho_c = 5330$ kg m^{-3}) and those using $\rho_c = 7800$ kg m^{-3} is of the order of 10^{-3}. Such a small difference does not change our conclusions.

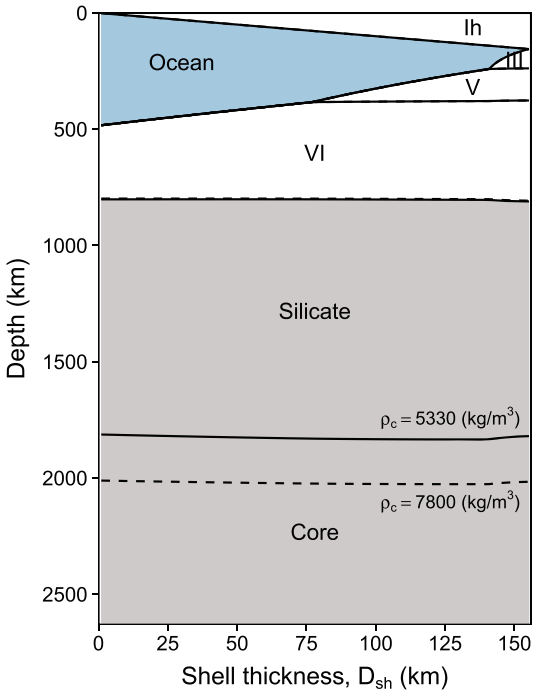

Figure 2. Our interior structure model for different shell thicknesses (D_{sh}). Solid and dashed curves show results for the core density ρ_c of 5330 and 7800 kg m^{-3}, respectively. The difference in ρ_c strongly affects the radius of the core. See Table 1 for parameters adopted.

Although the uncertainty in the density of the silicate mantle is much smaller than that of the metallic core, we found that the Love numbers are most sensitive to the mantle density compared to other parameters describing the deep interior (i.e., the rocky mantle and the metallic core); a 200 kg m^{-3} difference in the mantle density can lead to differences in $|h_2|$ and $|k_2|$ up to ~0.11 and ~0.043, respectively. Since typical $|h_2|$ and $|k_2|$ are about 1 and 0.5, respectively, these differences are about 10% of the Love numbers. Such large differences, however, can be found only under specific conditions and thus do not change our conclusions (see Appendix A).

2.2. Rigidity

The rigidity of ices has been investigated experimentally by several studies. In this study, we assume that each layer has a uniform rigidity since the pressure and temperature dependencies of rigidity are much weaker than those of density and of viscosity [e.g., *Schulson and Duval*, 2009]. Nevertheless, rigidity of the ice Ih shell may be the major control on tidal deformation of icy satellites [*Moore and Schubert*, 2000], and a small change in rigidity due to porosity or contaminants may have nonnegligible effects [e.g., *Hessinger et al.*, 1996]. To quantify such an effect, rigidity of the top shell (μ_{sh}) is treated as a free parameter.

On the other hand, the rigidity of the rocky mantle is fixed in this study. We found that the use of different values of rigidity for the mantle (i.e., 50 GPa and 120 GPa) leads to differences in $|h_2| < 0.01$ and that such a small difference does not change our conclusions.

It is also noted that we assume an inviscid fluid core; zero rigidity is assumed. We found that Love numbers for a model with a solid core are almost the same as those for our nominal model; an interior structure model having a purely elastic core, whose rigidity is 100 GPa, leads to the difference in $|h_2|$ only less than ~0.01. Consequently, the use of a solid core model does not change our conclusions.

2.3. Viscosity

In this study, we assume a flow law of pure water ice and a thermally convective ice Ih shell. More specifically, the viscosity η of the ice Ih shell is calculated from the following equation:

$$\eta(r) = \eta_{\mathrm{ref}} \exp\left[\frac{E_a}{R_g T_m(P)}\left(\frac{T_m(P)}{T(r)} - 1\right)\right], \tag{5}$$

where $T_m(P)$ is the pressure-dependent melting point, E_a is the activation energy, and R_g is the gas constant, respectively [e.g., *Tobie et al.*, 2005a]. We use $E_a = 60$ kJ mol^{-1} for pure water ice [*Goldsby and Kohlstedt*, 2001]. The thermal profile is calculated using a parameterized convection model. Here we adopt a scaling law between the Rayleigh number (*Ra*) and Nusselt number (*Nu*) for a bottom heated spherical shell incorporating the effect of curvature and the temperature dependence of viscosity [*Yao et al.*, 2014]:

$$Nu = \frac{1.46 Ra^{0.27}}{\gamma^{1.21} f^{0.78}}, \tag{6}$$

where γ is a parameter describing the temperature dependence of viscosity given by

$$\gamma = \frac{E_a\left(T_m(P) - T_s\right)}{R_g T_c^2} \tag{7}$$

and $f = 1 - D_{sh}/R_s$ is curvature, respectively. Here R_s is the radius of Ganymede, and T_s is the surface temperature. T_c is the temperature of the convective region calculated from

$$T_c = T_m(P) - \frac{1.23 R_g T_c^2}{f^{1.5} E_a}. \tag{8}$$

Parameter values required for determining *Ra* and *Nu* are listed in Table 1. For cases without a subsurface ocean, we adopt a basal temperature of 250 K for the ice Ih shell and obtained the viscosity profile following the procedure described above. It is noted that we assume that the convective region has a constant temperature T_c; a temperature increase with the adiabatic temperature gradient is ignored. Since, the adiabatic temperature gradient in the shell is sufficiently small (i.e., $\alpha g T/C_p \sim 10^{-2}$ K/km), it has little effect on the temperature and the viscosity profile.

Figure 3 shows temperature and viscosity profiles of the ice Ih shell for $D_{sh} = 100$ km. For this case, thermal convection occurs if $\eta_{ref} < 10^{17}$ Pa s because of the thick shell. The viscosity near the surface is much higher

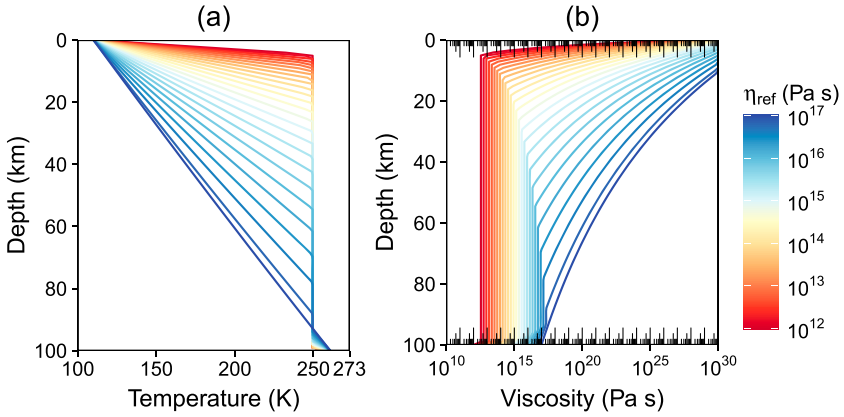

Figure 3. (a) Temperature and (b) viscosity profiles of the top ice Ih shell for different reference viscosities (η_{ref}). Results for shell thickness $D_{sh} = 100$ km are shown. Because of the thick shell, thermal convection occurs for most cases, leading to a constant temperature and viscosity region.

than that for the convective region because of the low surface temperature. In this study, such strongly depth-dependent viscosity profiles for the ice Ih shell are employed.

On the other hand, we assume that each HP ice layers and the rocky mantle have a uniform viscosity profile. Since rheologies of HP ices under a low-stress condition are highly uncertain [e.g., *Kubo et al.*, 2006], we consider a wide range of the viscosity for the HP ice layer (i.e., 10^{12}–10^{17} Pa s). For cases without an ocean, the viscosity for ice III (η_{III}), ice V (η_V), and ice VI (η_{VI}) are assumed to be independent free parameters. On the other hand, for cases with an ocean, these viscosities are assumed to be the same and denoted as $\eta_{HP} (= \eta_{III} = \eta_V = \eta_{VI})$.

It is noted that our nominal model assumes a viscosity of 10^{21} Pa s for the rocky mantle. We found that the use of different values of viscosity for the mantle (i.e., 10^{19} Pa s and 10^{23} Pa s) leads to differences in $|h_2| < 10^{-4}$ and that such a small difference does not change our conclusions.

2.4. Free Parameters

Here we summarize the free parameters in this study. For cases with a subsurface ocean, there are four free parameters: the thickness of the shell (D_{sh}), the rigidity of the ice Ih (μ_{sh}), the reference viscosity of ice Ih (η_{ref}), and the viscosity of HP ices (η_{HP}). We use 155 different values for D_{sh}, ranging from 1 to 155 km; the interval is uniformly 1 km. For μ_{sh}, we use 100 different values, ranging from 0.1 to 10 GPa; the interval is uniformly 0.1 GPa. For η_{ref}, we use 101 different values, ranging from 10^{12} to 10^{17} Pa s; the interval is uniformly 0.05 in terms of common logarithms. For η_{HP}, we use six different values, ranging from 10^{12} to 10^{17} Pa s; the interval is uniformly 1 in terms of common logarithms. Thus, we consider $155 \times 100 \times 101 \times 6 = 9,393,000$ cases.

For cases without a subsurface ocean, there are five free parameters: the rigidity of the ice Ih (μ_{sh}), the reference viscosity of ice Ih (η_{ref}), and the viscosity of HP ices ($\eta_{III}, \eta_V, \eta_{VI}$). For μ_{sh}, we use 34 different values, ranging from 0.1 to 10 GPa; the interval is uniformly 0.3 GPa. For viscosities, we use 26 different values, ranging from 10^{12} to 10^{17} Pa s; the interval is uniformly 0.2 in terms of common logarithms. Thus, we consider $34 \times 26 \times 26 \times 26 \times 26 = 15,537,184$ cases.

It is noted that above numbers of cases are for our nominal model. As discussed above, we conduct sensitivity checks for fixed parameters, such as the density of the core. Such additional calculations are not counted in above numbers.

3. Love Number Calculation Method

In a Ganymede reference frame, the time-dependent tidal potential Φ_t to first order in the eccentricity is given by

$$\Phi_t(r,\theta,\phi,t) = r^2\omega^2 e\left[-\frac{3}{2}P_2^0(\cos\theta)\cos\omega t + \frac{1}{4}P_2^2(\cos\theta)\{3\cos\omega t\cos 2\phi + 4\sin\omega t\sin 2\phi\}\right], \quad (9)$$

where ω is orbital angular frequency, e is eccentricity, t is time, θ is colatitude, ϕ is longitude with zero longitude at the sub-Jovian point, and P_n^m is the associated Legendre polynomial of degree n and of order m, respectively [e.g., *Kaula*, 1964]. Such a potential causes degree-2 deformation on a satellite. Thus, we calculate spheroidal degree-2 deformation using a spectral scheme which has been used in several previous studies [e.g., *Tobie et al.*, 2005b; *Wahr et al.*, 2009; *Kamata et al.*, 2015]. In the following, we briefly summarize the method. See *Kamata et al.* [2015] for further details.

The governing equation system consists of three equations; the equation of momentum conservation for a self-gravitating body given by

$$\rho\frac{\mathrm{d}^2\mathbf{u}}{\mathrm{d}t^2} = \boldsymbol{\nabla}\cdot\sigma + \rho\boldsymbol{\nabla}\Phi, \tag{10}$$

the Poisson equation for the gravitational field given by

$$\boldsymbol{\nabla}^2\Phi = 4\pi G\boldsymbol{\nabla}\cdot(\rho\mathbf{u}), \tag{11}$$

and the constitutive equation for a Maxwell body given by

$$\frac{\mathrm{d}\sigma_{ij}}{\mathrm{d}t} + \frac{\mu}{\eta}\left(\sigma_{ij} - \frac{\sigma_{kk}}{3}\delta_{ij}\right) = \lambda\frac{\mathrm{d}\varepsilon_{kk}}{\mathrm{d}t}\delta_{ij} + 2\mu\frac{\mathrm{d}\varepsilon_{ij}}{\mathrm{d}t}, \tag{12}$$

where $\mathbf{u}$ is the displacement vector, σ is the stress tensor, ε is the strain tensor, Φ is the gravitational potential, η is viscosity, μ is rigidity (i.e., shear modulus), $\lambda(=\kappa - 2\mu/3)$ is the first Lamé's parameter, and δ_{ij} is the unit diagonal tensor, respectively. The effect of bulk viscosity is not taken into account. For solid layers, applications of Fourier transformation in the time domain and spherical harmonic expansion in the spatial domain lead to a six-component first-order differential equation system:

$$\frac{\mathrm{d}y_i(n,r)}{\mathrm{d}r} = \sum_{j=1}^{6} A_{ij}(n,r)y_j(n,r) \quad (i,j = 1,2,\ldots,6), \tag{13}$$

where n is spherical harmonic degree, y_1 is the coefficient for the vertical displacement, y_2 is that for the vertical stress, y_3 is that for the tangential displacement, y_4 is that for the tangential stress, y_5 is that for the gravitational potential perturbation, and y_6 is that for the "potential stress." The matrix A is a function of the interior structure model, i.e., $\rho(r)$, $\mu(r)$, $\kappa(r)$, $\eta(r)$, and the frequency of potential perturbation, ω. Similarly, a four-component first-order differential equation system is obtained for a liquid layer which has $\mu = 0$ [e.g., *Takeuchi and Saito*, 1972; *Kamata et al.*, 2015]. One can integrate equation (13) using a numerical integration scheme and obtain linearly independent solutions. The coefficients for such solutions can be determined from the boundary conditions at the surface, layer boundaries, and the center.

Nondimensional complex Love numbers can be written using the solution y at the surface; the degree-2 displacement Love number h_2 and potential Love number k_2 are given by

$$h_2 = g_s y_1(n=2, r=R_s)/\tilde{\Phi}_t(n=2) \tag{14}$$

$$k_2 = y_5(n=2, r=R_s)/\tilde{\Phi}_t(n=2) - 1 \tag{15}$$

where g_s is the gravitational acceleration at the surface and $\tilde{\Phi}_t(n)$ is the degree-n coefficient of tidal potential. Note that y (and thus h_2 and k_2) is a complex variable, and the absolute value and argument yield the amplitude and phase shift, respectively.

4. Results and Discussion

We first consider how to infer the presence/absence of a subsurface ocean based on Love numbers. We then investigate the major control on tidal response to understand what information we can obtain from Love numbers. We find that it is the thickness of the ice Ih shell if Ganymede possesses a subsurface ocean, though a precise estimate of the shell thickness may be difficult if we use either of h_2 or k_2 alone. Finally, we consider how well we can constrain the shell thickness if we use both h_2 and k_2.

4.1. The Presence/Absence of a Subsurface Ocean

Figure 4 shows the relation between the absolute values of h_2 and k_2. For cases with a subsurface ocean, $|h_2|$ and $|k_2|$ range about 1.1–1.7 and about 0.36–0.57, respectively. These values are consistent with those

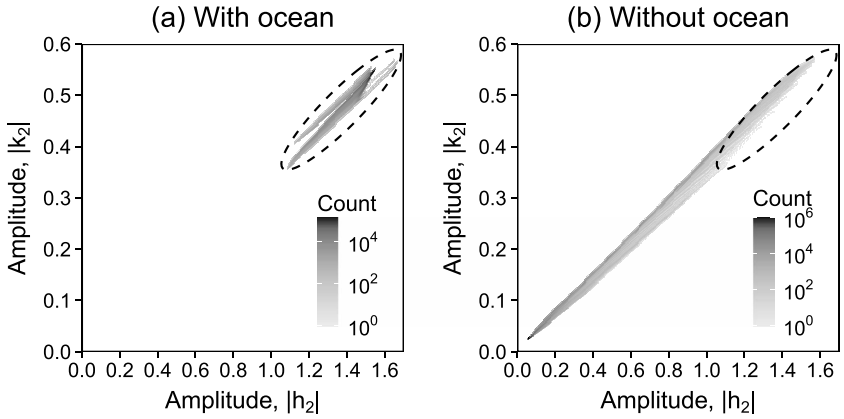

Figure 4. Two-dimensional histogram of the tidal amplitude for (a) cases with a subsurface ocean and for (b) cases without a subsurface ocean. The horizontal and vertical axes represent the absolute value of the displacement Love number (h_2) and that of the potential Love number (k_2), respectively. The dashed oval represents the distribution of solutions for cases with an ocean.

obtained by previous studies [e.g., *Moore and Schubert*, 2003; *Steinbrügge et al.*, 2015]. A model with a larger $|h_2|$ tends to have a larger $|k_2|$, indicating that such a model has a softer ice shell. This trend is also the case for models without a subsurface ocean. The ranges of Love numbers, however, are clearly different between cases with and without an ocean; the latter model covers much wider ranges, $|h_2|$ of 0.05 – 1.6 and $|k_2|$ of 0.03 – 0.57, respectively. This result is also consistent with those obtained by a previous study [*Moore and Schubert*, 2003]. Comparing these results, it can safely be said that if future geodetic observations yield $|h_2| < 1$ or $|k_2| < 0.35$, Ganymede does not possess a subsurface ocean. On the other hand, large Love numbers (i.e., $|h_2| > 1$ or $|k_2| > 0.35$) can be seen not only for cases with an ocean but also for those without an ocean (dashed ovals in Figure 4). Consequently, if a large tidal amplitude is observed, it would be difficult to infer whether Ganymede possesses a subsurface ocean or not in the absence of other constraints.

Nevertheless, this result does not necessarily indicate that geodetic measurements cannot infer the presence/absence of a subsurface ocean in Ganymede. We found that the phase lag of tidal deformation is a key to determine the presence/absence of a subsurface ocean. Figure 5 shows the relation between the amplitude and phase lag for k_2. A phase lag only as large as 12° is found for cases with an ocean. On the other hand, cases without an ocean generally have large phase lags up to about 65°. While a small phase lag (i.e., <10°) is also found for cases without an ocean, such a model mostly accompanies a small amplitude (i.e., $|k_2| < 0.1$). Such a small amplitude is not obtained for cases with an ocean. Consequently, measurements of the phase lag as well as the amplitude provide critical information for the presence/absence of a subsurface ocean.

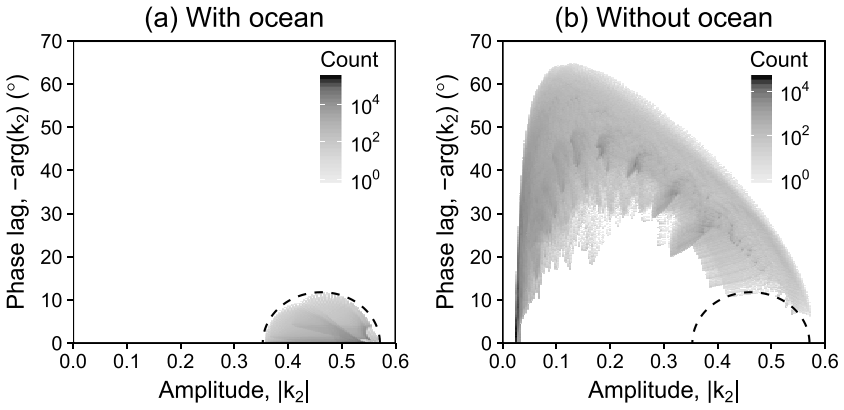

Figure 5. Two-dimensional histogram of the gravitational tidal response for (a) cases with a subsurface ocean and for (b) cases without a subsurface ocean. The horizontal and vertical axes represent the absolute value and the argument of the potential Love number (k_2), respectively. The dashed oval represents the distribution of solutions for cases with an ocean.

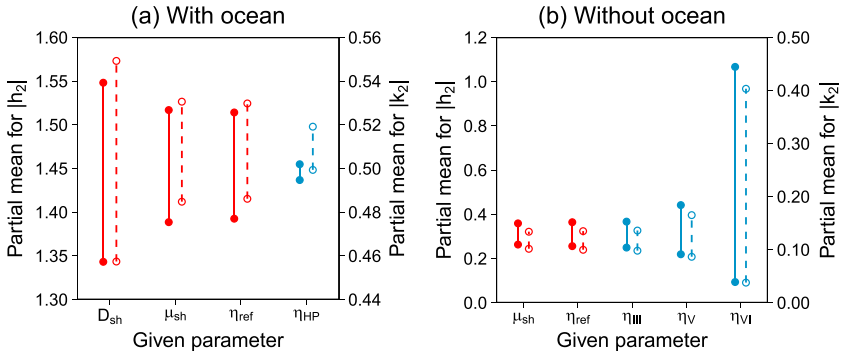

Figure 6. Partial mean values of the absolute value of Love numbers for (a) cases with a subsurface ocean and for (b) cases without a subsurface ocean. Results for $|h_2|$ are shown using solid lines and closed circles, while those for $|k_2|$ are shown using dashed lines and open circles. Red and blue lines and symbols are variables for the ice Ih shell and for high-pressure ice layers, respectively. The factor that leads to the largest variation in partial means is D_{sh} for Figure 6a and η_{VI} for Figure 6b.

We note that this argument is also applicable to h_2; cases with an ocean have phase lags $< \sim 10°$, and cases without an ocean having such small phase lags mostly accompany $|h_2| < 0.2$.

The detectability of phase lag is not clear particularly for h_2. However, *Parisi et al.* [2014] argue that gravity field measurements with a low altitude would provide k_2 with an absolute accuracy of about 10^{-3}, both for real and imaginary parts. The imaginary part of k_2 is given by $-|k_2| \sin(\phi_{lag}) \approx -|k_2|\phi_{lag}$, where ϕ_{lag} is phase lag and is a small value. Consequently, if $|k_2| = 0.5$ and $\phi_{lag} = 1°$, the imaginary part of k_2 is ~0.01. Thus, precise gravity field measurements can lead to the determination precision of the phase lag of the order of 1° or better. We thus conclude that geodetic measurements during the JUICE mission would have a sufficient precision to infer the presence/absence of a subsurface ocean.

4.2. Major Control on Tidal Response

In addition to the presence/absence of a subsurface ocean, what kind of information can we obtain from the tidal response? In other words, what is the major control on the tidal response of Ganymede? To answer this question quantitatively, we analyze our results using partial means. Consider a variable X which is a function of Y and Z, and Y is the major control on X. Under such a situation, the partial means of X for a given Y_i,

$$\bar{X}(Y_i) = \frac{1}{j_{max}} \sum_{j=1}^{j_{max}} X(Y_i, Z_j), \tag{16}$$

depend strongly on the choice of Y_i because Y is the major control on X. On the other hand, the partial means for a given Z_i,

$$\bar{X}(Z_i) = \frac{1}{j_{max}} \sum_{j=1}^{j_{max}} X(Y_j, Z_i), \tag{17}$$

depend little on the choice of Z_i because Z is the minor control on X. Thus, the factor that leads to the largest variation in partial means is the major control.

Figure 6 shows variations in partial means for the absolute value of Love numbers. For cases with a subsurface ocean, we find that the thickness of the ice Ih shell (D_{sh}) gives the largest variation in partial means for $|h_2|$ and $|k_2|$. Consequently, the major control on tidal response is the thickness of the ice Ih shell. On the other hand, for cases without a subsurface ocean, we find that the major control is the viscosity of the ice VI layer, which is the deepest and thickest H_2O layer (see Figure 2).

It should be noted that the dependence of Love numbers on D_{sh} is not linear; Love numbers decrease with increasing shell thickness if $D_{sh} \leq 152$ km, though Love numbers increase if $D_{sh} \geq 152$ km. The former trend indicates that a thicker shell is more resistant to deformation. The latter, counterintuitive result is caused by tidal resonance; a thin ocean having a gravity wave speed close to the phase velocity of degree-2 deformation enhances tidal deformation [e.g., *Kamata et al.*, 2015].

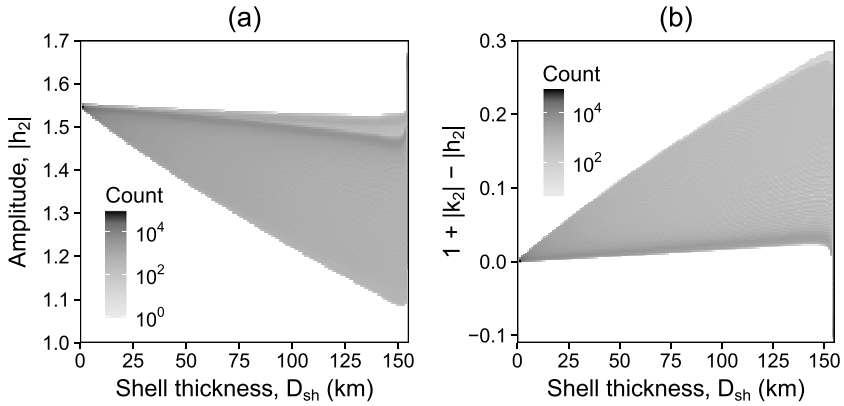

Figure 7. Two-dimensional histogram of (a) tidal amplitude ($|h_2|$) and of (b) a linear combination of Love numbers as functions of shell thickness (D_{sh}). A thin and a thick shell have small and large variations in $|h_2|$ and $1 + |k_2| - |h_2|$.

4.3. Estimation of the Thickness of the Ice Ih Shell

Although the thickness of the ice Ih shell is the major control on the amplitude of tidal response (if Ganymede possesses a subsurface ocean), unfortunately this does not necessarily indicate that measurements of either of $|h_2|$ or $|k_2|$ alone are sufficient to estimate the thickness of the ice Ih shell precisely. Figure 7a shows the range of $|h_2|$ as a function of D_{sh}. If D_{sh} is small, the range of $|h_2|$ is small independent of other parameters. As D_{sh} increases, the range of $|h_2|$ increases, indicating that other parameters have a larger effect on the tidal response. If $D_{sh} = 155$ km, the thickness of the subsurface ocean is <1 km, leading to an enhanced $|h_2|$ due to tidal resonance [*Kamata et al.*, 2015]. We found the same trends for $|k_2|$: a small D_{sh} leads to $|k_2| \sim 0.55$, while a large D_{sh} leads to $0.36 < |k_2| < 0.56$, and $D_{sh} = 155$ km could lead to $|k_2| > 0.56$.

In terms of shell thickness estimation based on Love numbers, these results indicate that (1) if a small tidal amplitude (for example, $|h_2| = 1.1$) is observed, the ice Ih shell is thick (i.e., $D_{sh} \sim 150$ km), and that (2) if $|h_2| > 1.6$ is observed, $D_{sh} > 154$ km; a thin ocean beneath a thick shell leads to tidal resonance. The problem is that if we observe a relatively large amplitude, such as $|h_2| \sim 1.5$, it is difficult to estimate the thickness of the ice Ih shell.

One might argue that such a large uncertainty could be reduced by using a linear combination of Love numbers. *Wahr et al.* [2006] consider tidal deformation on Europa and show that $1 + |k_2| - |h_2|$ linearly depends on shell thickness and thus could be a good index for shell thickness. *Steinbrügge et al.* [2015] show that this is also the case for Ganymede. These works, however, use fully elastic models with a given ice rigidity. We found that different viscosities and/or rigidities lead to a different $1 + |k_2| - |h_2|$ for a given D_{sh}, as shown in Figure 7b. Thus, the use of this linear combination of Love numbers would not reduce the uncertainty in the shell thickness unless we assume the viscosity and rigidity of the ice Ih shell.

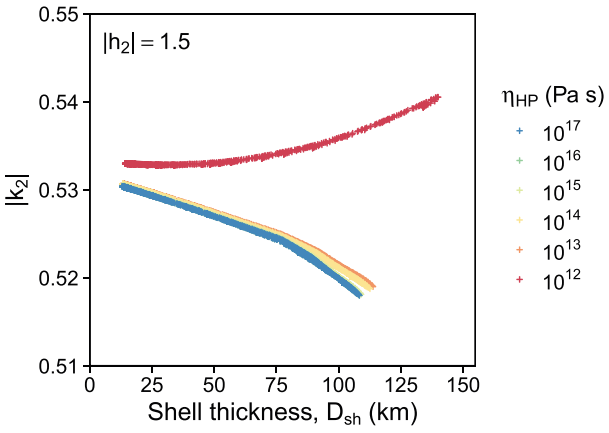

Figure 8. The absolute value of k_2 as a function of shell thickness (D_{sh}) for a given $|h_2|$. If $|h_2|$ and η_{HP} is given, $|k_2|$ is a good index for D_{sh} independent of μ_{sh} and η_{ref}.

Nevertheless, the use of both $|h_2|$ and $|k_2|$ can reduce the uncertainty in the shell thickness. Figure 8 shows the relation between D_{sh} and $|k_2|$ for a given $|h_2|$. Results for all the ranges of η_{ref}, μ_{sh}, and η_{HP} are shown. For a given η_{HP}, $|k_2|$ monotonically changes with increasing D_{sh} (if we fix $|h_2|$). See Appendix B for an explanation for the trends. Figure 8 indicates that if we can constrain the viscosity of HP ices, precise measurements of $|h_2|$ and $|k_2|$ enable us to determine the thickness

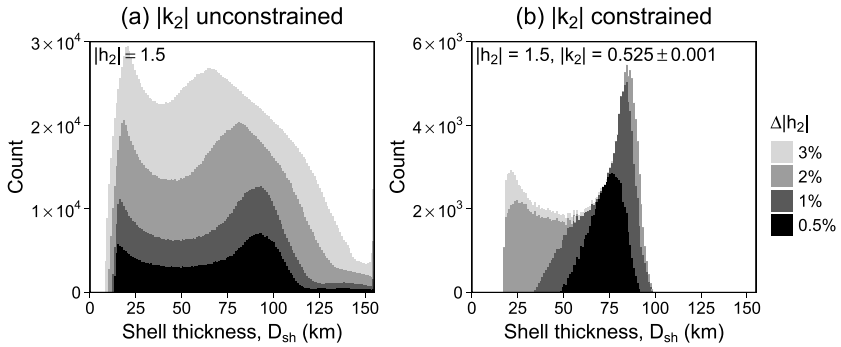

Figure 9. Histogram of the thickness of the ice Ih shell (D_{sh}) for a given $|h_2|$ with different errors. Results under conditions where $|k_2|$ is (a) unconstrained and (b) constrained. The increase in the precision of $|h_2|$ decreases the uncertainty in the shell thickness only if $|k_2|$ is constrained.

of the ice Ih shell precisely. Consequently, in addition to the precise determination of $|h_2|$ and $|k_2|$, studies of high-pressure ice rheologies and detailed thermal modeling of the deep interior of Ganymede are important for constraining the structure of the upper part of Ganymede. For ice II, the effective viscosity under a low-stress condition can be smaller even by several orders of magnitude than that for ice Ih [*Kubo et al.*, 2006]. Our results indicate that whether a viscosity $<10^{13}$ Pa s is plausible for HP ices or not under the conditions relevant to Ganymede is an important subject to be investigated.

Actual tidal deformation measurements cannot avoid including some errors. Figure 9 shows the uncertainty in the shell thickness with plausible ranges of errors in $|h_2|$. As already seen in Figure 7a, the uncertainty in D_{sh} is extremely large if $|h_2| \sim 1.5$. Consequently, a decrease in the error for $|h_2|$ does not lead to a decrease in the uncertainty in D_{sh} (Figure 9a). However, as noted above, $|k_2|$ depends strongly on D_{sh} for a given $|h_2|$. We found that a decrease in the error for $|h_2|$ leads to a decrease in the uncertainty in D_{sh} if $|k_2|$ is constrained (Figure 9b). The nominal error in the $|h_2|$ measurements using Ganymede Laser Altimeter (GALA) on board the JUICE spacecraft is ~2% and decreases with increasing number of crossover points [*Steinbrügge et al.*, 2015]. Thus, our results highlight the importance of an extended mission for altimetric measurements as well as of collaborative analyses of topography and gravity field data for constraining the interior structure of Ganymede.

4.4. Discussion

Our results indicate that the tidal amplitude does not have a one-to-one correspondence with the shell thickness; a thick shell leads to a wide range of $|h_2|$ and $|k_2|$ depending on the property of the ice Ih shell (section 4.3). One might argue that the tidal amplitude is controlled not by the thickness of the shell but by the thickness of the lithosphere or the heat flux. Figure 10 compares the tidal response and the thickness of the lithosphere (i.e., the layer with a viscosity higher than 10^{25} Pa s) and the surface heat flux, illustrating that the tidal amplitude does not have a one-to-one correspondence with these parameters either. Thus, it would be difficult to constrain the lithospheric thickness and the heat flux from the tidal amplitude. On the other hand, phase lag can be large only if the lithospheric thickness is ~5 km and the surface heat flux is ~15 mW m^{-2}. Consequently, if we observe a phase lag of ~8° and $|h_2|$ of >1, it would imply the presence of a subsurface ocean as well as a lithospheric thickness of ~5 km. Nevertheless, if we observe a small phase lag (i.e., <2°), we can constrain neither of the thickness of the lithosphere nor the heat flux.

In the following, we consider the validity of our model assumptions. The major simplification in our model is that we assume a pure H_2O ocean. If the ocean contains other molecules, such as ammonia, the melting temperature (i.e., the basal temperature) is lower than our model [e.g., *Choukroun and Grasset*, 2010]. This would lead to a decrease in temperature and an increase in the viscosity of the ice shell. However, as discussed above, the viscosity of the ice Ih shell is not the major control on the tidal response of Ganymede. In addition to the melting temperature, the density of the ocean also depends on its chemical composition. Although its effect on the tidal response is not completely zero, it should be small since the properties of the ice Ih shell largely determine the tidal response. Thus, while the quantification of these effects requires further detailed modeling using a phase diagram of nonpure water ice and different thermophysical models, our results would not change significantly.

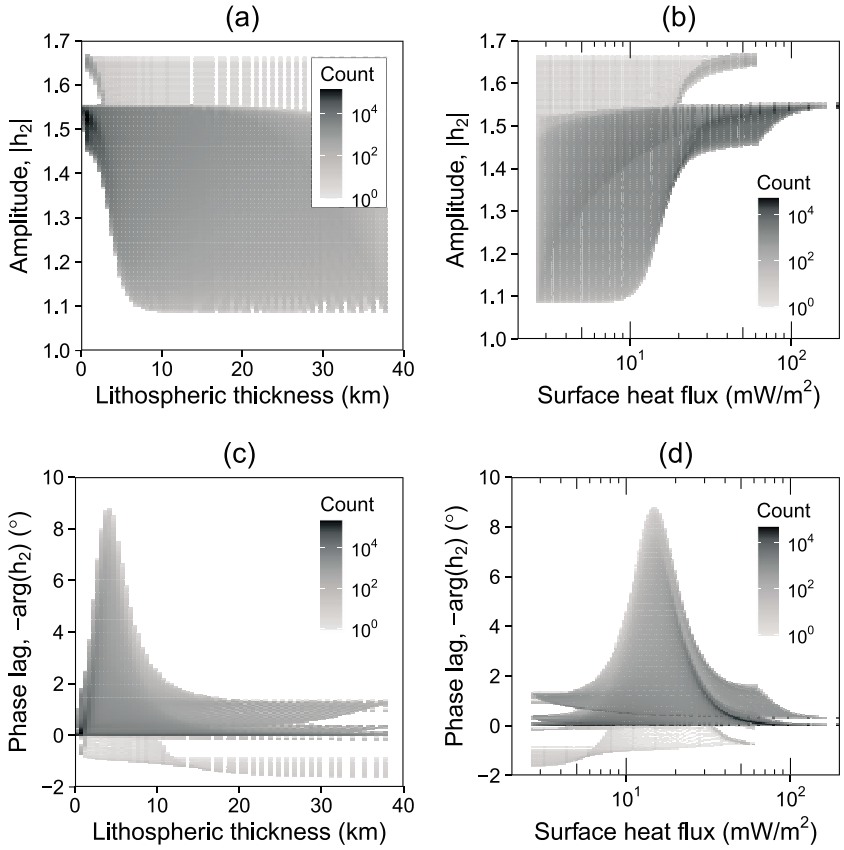

Figure 10. Two-dimensional histogram of (a) lithospheric thickness versus tidal amplitude, (b) surface heat flux versus tidal amplitude, (c) lithospheric thickness versus phase lag, and (d) surface heat flux versus phase lag.

Another simplification adopted in this study is the rheology of the ice shell. The presence of other volatiles, such as CO_2 and CH_4, may change the viscosity of ice [e.g., *Durham et al.*, 2010], though we explored a wide range of the reference viscosity and found that it is not the major control on tidal response.

In our model, an increased activation energy (leading to an enhanced deformation rate) at a high temperature (i.e., >258 K) seen in laboratory experiments [*Goldsby and Kohlstedt*, 2001] is not incorporated. Furthermore, the temperature dependence of thermal conductivity and other parameters for ice Ih are not considered. This is because the *Ra-Nu* scaling law we adopt is based on models which neglect these effects. For further detailed modeling, development of a *Ra-Nu* scaling law incorporating these effects is necessary.

5. Conclusion

We modeled the tidal response of Ganymede adopting a realistic interior structure model considering a convective ice shell and investigated its parameter dependence. Cases with a subsurface ocean lead to large tidal amplitudes, while those without a subsurface ocean can lead to a wide range of the tidal amplitude depending mainly on the viscosity of the ice VI layer. Because of this, it is difficult to infer whether Ganymede possesses a subsurface ocean or not based only on the amplitude of tidal deformation. In contrast, the phase lag is different between cases with and without an ocean; models with an ocean have phase lags smaller than models without an ocean. Consequently, the determination of the phase lag as well as the tidal amplitude is critical to infer the presence/absence of a subsurface ocean in Ganymede. If a subsurface ocean exists, the major control on tidal response is the thickness of the ice Ih shell. To estimate the thickness of this shell precisely, constraints on both of the Love numbers, h_2 and k_2, with a high accuracy is necessary. This result indicates the importance of an extended mission time as well as of data analyses using both of topography and gravity field data.

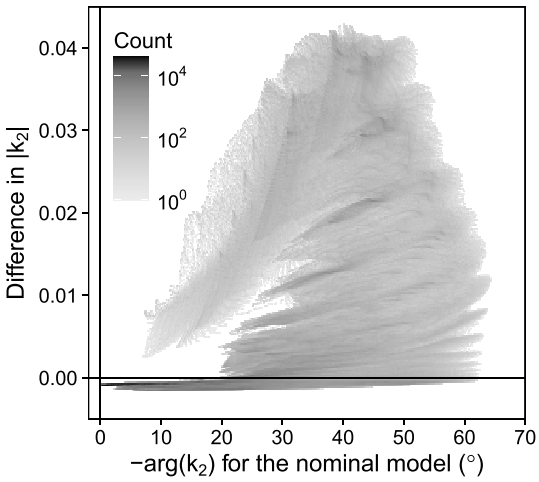

Figure A1. Difference in $|k_2|$ between our nominal model (i.e., $\rho_m = 3222$ kg m^{-3}) and models with $\rho_m = 3022$ kg m^{-3}. Results for cases without a subsurface ocean are shown. A large difference can be found only for cases with a large phase lag.

Appendix A: Different Rocky Mantle Densities

A change in the mantle density affects the depths of boundaries between the ice VI layer and the rocky mantle and between the rocky mantle and the metallic core. Consequently, the mantle density controls the thickness of the ice VI layer. This is because the mean density and the moment of inertia for our model need to match the observed values. As discussed in section 4.2, the viscosity of this deep ice layer is the major control on tidal response if a subsurface ocean does not exist. Because of this, the use of a different mantle density could lead to nonnegligible contributions to the tidal response for cases without an ocean.

However, the tidal response for cases with a subsurface ocean is almost independent of the mantle density. In addition, cases without an ocean and with a small phase lag (i.e., <10°) have small difference in Love numbers (i.e., $\Delta|k_2| <\sim 0.01$) between models using different mantle densities, as seen in Figure A1. Consequently, even if we adopt different mantle densities, solutions for cases with an ocean remain confined in the dashed region in Figure 5, while most solutions for cases without an ocean are distributed outside the dashed region in the figure. Thus, the use of different mantle densities does not affect our conclusion that the determination of the phase lag as well as the amplitude is a key to infer whether Ganymede possesses a subsurface ocean or not.

Appendix B: Trends of $|k_2|$ as a Function of D_{sh} Under a Given $|h_2|$

Here we examine what determines the trends of $|k_2|$ as a function of D_{sh} under a given $|h_2|$ seen in Figure 8. Deformation of density boundaries produces gravity anomalies, but how it contributes to $|k_2|$ depends both on the amplitude and on the depth; a larger amplitude and a shallower boundary lead to a larger $|k_2|$.

Figure B1 shows the amplitudes of deformation at three different depths: surface, the base of the ice Ih shell, and the top of the high-pressure (HP) ice layer. Since we consider models which give $|h_2| = 1.5$, the amplitude of surface deformation is fixed. The amplitude of deformation at the base of the ice Ih shell is close to that at the surface and is nearly independent of η_{HP} nor D_{sh}. While the amplitude does not vary significantly, its depth increases with increasing D_{sh}, leading to a smaller contribution to $|k_2|$ with increasing D_{sh}. This causes the decrease in $|k_2|$ with increasing D_{sh} for $\eta_{HP} = 10^{13}$ Pa s (see Figure 8).

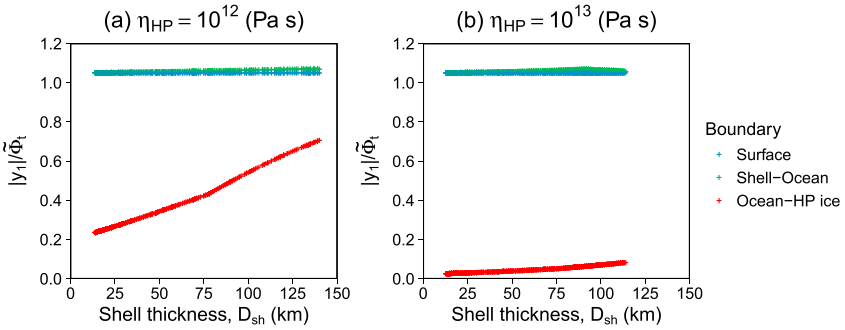

Figure B1. Amplitude of vertical displacement $|y_1|$ normalized by tidal potential $\tilde{\Phi}_t$. Results for three different depths (i.e., the surface, the base of the ice Ih shell, and the top of the HP ice layer) are shown.

On the other hand, the amplitude of deformation at the top of HP ice layer depends on η_{HP}; if $\eta_{HP} \geq 10^{13}$ Pa s, the HP ice layers are relatively highly viscous, so that the ocean-HP ice boundary does not deform significantly. In contrast, if $\eta_{HP} \leq 10^{12}$ Pa s, the ocean-HP ice boundary deforms because of a low HP ice viscosity. Since a thinner ocean leads to a stronger gravitational coupling between the ice Ih shell and the HP ice layers, a larger deformation occurs for a larger D_{sh}. This causes the increase in $|k_2|$ with increasing D_{sh} for $\eta_{HP} = 10^{12}$ Pa s (see Figure 8).

Acknowledgments
We thank Michael Efroimsky and an anonymous reviewer for their careful reviews and constructive comments and Steven A. Hauck II for comments improving the manuscript. No actual field data are used. Any requests for data produced in this study should be sent to Shunichi Kamata at kamata@mail.sci.hokudai.ac.jp. This work was partially supported by JSPS KAKENHI grant 16K17787.

References

A, G., J. Wahr, and S. Zhong (2014), The effects of laterally varying icy shell structure on the tidal response of Ganymede and Europa, *J. Geophys. Res. Planets*, *119*, 659–678, doi:10.1002/2013JE004570.

Bland, M. T., A. P. Showman, and G. Tobie (2009), The orbital-thermal evolution and global expansion of Ganymede, *Icarus*, *200*, 207–221, doi:10.1016/j.icarus.2008.11.016.

Choukroun, M., and O. Grasset (2010), Thermodynamic data and modeling of the water and ammonia-water phase diagrams up to 2.2 GPa for planetary geophysics, *J. Chem. Phys.*, *133*, 144502, doi:10.1063/1.3487520.

Durham, W. B., O. Prieto-Ballesteros, D. L. Goldsby, and J. S. Kargel (2010), Rheological and thermal properties of icy materials, *Space Sci. Rev.*, *153*, 273–298, doi:10.1007/s11214-009-9619-1.

Goldsby, D. L., and D. L. Kohlstedt (2001), Superplastic deformation of ice: Experimental observations, *J. Geophys. Res.*, *106*, 11,017–11,030, doi:10.1029/2000JB900336.

Grasset, O., et al. (2013), JUpiter ICy moons Explorer (JUICE): An ESA mission to orbit Ganymede and to characterise the Jupiter system, *Planet. Space Sci.*, *78*, 1–21, doi:10.1016/j.pss.2012.12.002.

Hessinger, J., B. E. White Jr., and R. O. Pohl (1996), Elastic properties of amorphous and crystalline ice films, *Planet. Space Sci.*, *44*, 937–944, doi:10.1016/0032-0633(95)00112-3.

Hussmann, H., G. Choblet, V. Lainey, D. L. Matson, C. Sotin, G. Tobie, and T. Van Hoolst (2010), Implications of rotation, orbital states, energy sources, and heat transport for internal processes in icy satellites, *Space Sci. Rev.*, *153*, 317–348, doi:10.1007/s11214-010-9636-0.

Kamata, S., I. Matsuyama, and F. Nimmo (2015), Tidal resonance in icy satellites with subsurface oceans, *J. Geophys. Res. Planets*, *120*, 1528–1542, doi:10.1002/2015JE004821.

Kaula, W. M. (1964), Tidal dissipation by solid friction and the resulting orbital evolution, *Rev. Geophys.*, *2*, 661–685, doi:10.1029/RG002i004p00661.

Kimura, J., T. Nakagawa, and K. Kurita (2009), Size and compositional constraints of Ganymede's metallic core for driving an active dynamo, *Icarus*, *202*, 216–224, doi:10.1016/j.icarus.2009.02.026.

Kivelson, M. G., K. K. Khurana, and M. Volwerk (2002), The permanent and inductive magnetic moments of Ganymede, *Icarus*, *157*, 507–522, doi:10.1006/icar.2002.6834.

Kubo, T., W. B. Durham, L. A. Stern, and S. H. Kirby (2006), Grain size-sensitive creep in ice II, *Science*, *311*, 1267–1269, doi:10.1126/science.1121296.

Lewis, J. S. (1995), *Physics and Chemistry of the Solar System*, Acad. Press, San Diego, Calif.

Moore, W. B., and G. Schubert (2000), The tidal response of Europa, *Icarus*, *147*, 317–319, doi:10.1006/icar.2000.6460.

Moore, W. B., and G. Schubert (2003), The tidal response of Ganymede and Callisto with and without liquid water oceans, *Icarus*, *166*, 223–226, doi:10.1016/j.icarus.2003.07.001.

Parisi, M., L. Iess, and S. Finocchiaro (2014), The gravity fields of Ganymede, Callisto and Europa: How well can JUICE do?, *Geophys. Res. Abstr. EGU2014*, 11758.

Saur, J., et al. (2015), The search for a subsurface ocean in Ganymede with Hubble Space Telescope observations of its auroral ovals, *J. Geophys. Res. Space Physics*, *120*, 1715–1737, doi:10.1002/2014JA020778.

Schubert, G., J. Anderson, T. Spohn, and W. McKinnon (2004), Interior composition, structure and dynamics of the Galilean satellites, in *Jupiter: The Planet, Satellites and Magnetosphere*, edited by F. Bagenal, T. Dowling, and W. McKinnon, pp. 281–306, Cambridge Univ. Press, Cambridge, U. K.

Schulson, E. M., and P. Duval (2009), *Creep and Fracture of Ice*, Cambridge Univ. Press, Cambridge, U. K.

Showman, A. P., D. J. Stevenson, and R. Malhotra (1997), Coupled orbital and thermal evolution of Ganymede, *Icarus*, *129*, 367–383, doi:10.1006/icar.1997.5778.

Sohl, F., T. Spohn, D. Breuer, and K. Nagel (2002), Implications from Galileo observations on the interior structure and chemistry of the Galilean satellites, *Icarus*, *157*, 104–119, doi:10.1006/icar.2002.6828.

Sotin, C., and G. Tobie (2004), Internal structure and dynamics of the large icy satellites, *C. R. Physique*, *5*, 769–780, doi:10.1016/j.crhy.2004.08.001.

Spohn, T., and G. Schubert (2003), Oceans in the icy Galilean satellites of Jupiter?, *Icarus*, *161*, 456–467, doi:10.1016/S0019-1035(02)00048-9.

Steinbrügge, G., A. Stark, H. Hussmann, F. Sohl, and J. Oberst (2015), Measuring tidal deformations by laser altimetry. A performance model for the Ganymede Laser Altimeter, *Planet. Space Sci.*, *117*, 184–191, doi:10.1016/j.pss.2015.06.013.

Takeuchi, H., and M. Saito (1972), Seismic surface waves, *Methods Comput. Phys.*, *11*, 217–295.

Tobie, G., O. Grasset, J. I. Lunine, A. Mocquet, and C. Sotin (2005a), Titan's internal structure inferred from a coupled thermal-orbital model, *Icarus*, *175*, 496–502, doi:10.1016/j.icarus.2004.12.007.

Tobie, G., A. Mocquet, and C. Sotin (2005b), Tidal dissipation within large icy satellites: Applications to Europa and Titan, *Icarus*, *177*, 534–549, doi:10.1016/j.icarus.2005.04.006.

Wahr, J., Z. A. Selvans, M. E. Mullen, A. C. Barr, G. C. Collins, M. M. Selvans, and R. T. Pappalardo (2009), Modeling stresses on satellites due to nonsynchronous rotation and orbital eccentricity using gravitational potential theory, *Icarus*, *200*, 188–206, doi:10.1016/j.icarus.2008.11.002.

Wahr, J. M., M. T. Zuber, D. E. Smith, and J. I. Lunine (2006), Tides on Europa, and the thickness of Europa's icy shell, *J. Geophys. Res.*, *111*, E12005, doi:10.1029/2006JE002729.

Yao, C., F. Deschamps, J. P. Lowman, C. Sanchez-Valle, and P. J. Tackley (2014), Stagnant lid convection in bottom-heated thin 3-D spherical shells: Influence of curvature and implications for dwarf planets and icy moons, *J. Geophys. Res. Planets*, *119*, 1895–1913, doi:10.1002/2014JE004653.